Mineralogical Magazine (2019), **83**, 95–105
doi:10.1180/mgm.2018.146

CAMBRIDGE UNIVERSITY PRESS

Article

Apatite with lamellae of sulfide and other phases in ultrahigh-pressure eclogites from Nové Dvory, Moldanubian Zone, Czech Republic

Shah Wali Faryad[1]*, Radim Jedlicka[1] and Maria Perraki[2]

[1]Institute of Petrology and Structural Geology, Charles University, Prague, Albertov 12843, Czech Republic and [2]Department of Geo-Sciences, School of Mining and Metallurgical Engineering, National Technical University of Athens, 9 Heroon Politechniou St, GR-15773, Zografou (Athens), Greece

Abstract

Exsolution lamellae of baryte, Fe sulfides, Cu sulfides and Fe oxides were observed in apatite enclosed in garnet and omphacite and their intergranular spaces in ultrahigh-pressure eclogite in the Moldanubian Zone, Czech Republic. Micro-textural relations and compositional mapping of the apatite indicates a close relationship between the density of the exsolution lamellae and compositional domains that are rich in sulfur and iron. No relation between compositional domains and fluorine or chlorine content or any evidence of apatite metasomatisation was observed. On the basis of cathodoluminescence images, the compositional domains reflect sector zoning in apatite crystals by preferential uptake of elements due to differences in surface charge and morphology on the growth plane. It is concluded that the lamellae are products of exsolution in a closed system resulting from temperature decrease during metamorphism.

Keywords: apatite, sulfide and baryte exsolution lamellae, eclogite, Bohemian Massif

(Received 18 January 2018; accepted 15 July 2018)

Introduction

As an accessory phase, apatite ($Ca_5(F,Cl,OH)(PO_4)_3$) is among the most important minerals controlling trace-element variation in igneous and metamorphic rocks (e.g. Watson and Harrison, 1984; Cherniak, 2000; Spear and Pyle, 2002). Apatite has been defined as a supergroup of minerals that is divided into five groups on the basis of composition (Pasero, 2010). In this work we use the term apatite generally to refer to all Ca phosphates in the apatite group and for discussion of older papers. Because of its ability to incorporate and possibly concentrate a range of minor and trace elements, apatite is potentially a good indicator of *P-T-X* (pressure-temperature-composition) changes during magmatic and metamorphic processes (Korzhinsky, 1981; Yardley, 1985; Gottesmann and Wirth, 1997; Smith and Yardley, 1999; Sallet, 2000; Sun *et al.*, 2007). In metamorphic rocks, apatite occurs over a wide *P–T* range from very low-grade conditions through amphibolite to high-temperature granulite facies, and even to ultrahigh-pressure metamorphic rocks (e.g. Liou *et al.*, 1998). By changing the temperature and/or pressure conditions, the crystal structure of the host mineral with ions of minor and trace elements becomes unstable and those elements incorporate into various phases created by exsolution (unmixing) (Yund and McCallister, 1970; Liou *et al.*, 1998). Exsolution lamellae in apatite have been reported from several high- to ultrahigh-grade rocks (Chen *et al.*, 2006; Zeng *et al.*, 2006; Sun *et al.*, 2007; Liu *et al.*, 2009; Broska *et al.*, 2014), and are composed of crystallographically-orientated minerals such as: monazite; hematite; magnetite; baryte; pyrrhotite; anhydrite; and dolomite. In addition to their formation from the host apatite in a closed system (e.g. Sun *et al.*, 2007), they are interpreted to be as a result of metasomatic reaction (Harlov *et al.*, 2002; Harlov, 2015; Broska *et al.*, 2014).

In this paper, we present micro-textures of apatite with exsolution lamellae of various minerals in eclogite from the Moldanubian Zone in the Bohemian Massif. Using compositional maps of the host crystal and cathodoluminescence imaging, we document the relationship between the distribution of exsolution lamellae and compositional zoning of minor and trace elements. In addition to the question of a closed, or open system, the formation of apatite and exsolution within, we discuss the process of unmixing in relation to the *P-T* trajectory constrained for the host rocks (Faryad *et al.*, 2009; Faryad *et al.*, 2013*a*).

Geological setting

The Bohemian Massif is located at the eastern end of the European Variscan orogenic belt. It is formed by two zones (the Moldanubian and Saxothuringian) with high- to ultrahigh-pressure (HP-UHP) metamorphic rocks and two blocks (the Teplá-Barrandian and Brunovistulian) that are free of HP-UHP rocks (Fig. 1*a*). The Moldanubian Zone consists mostly of amphibolite- and granulite-facies metamorphic rocks that contain bodies of garnet and/or spinel peridotite and eclogite (for more information see Medaris *et al.*, 1990; Schulmann *et al.*, 2005; Faryad *et al.*, 2009; 2013*b*; Svojtka *et al.*, 2016). This zone is

*Author for correspondence: Shah Wali Faryad, Email: faryad@natur.cuni.cz
Associate Editor: Makoto Arima
Cite this article: Faryad S.W., Jedlicka R. and Perraki M. (2019) Apatite with lamellae of sulfide and other phases in ultrahigh-pressure eclogites from Nové Dvory, Moldanubian Zone, Czech Republic. *Mineralogical Magazine*, **83**, 95–105. https://doi.org/10.1180/mgm.2018.146

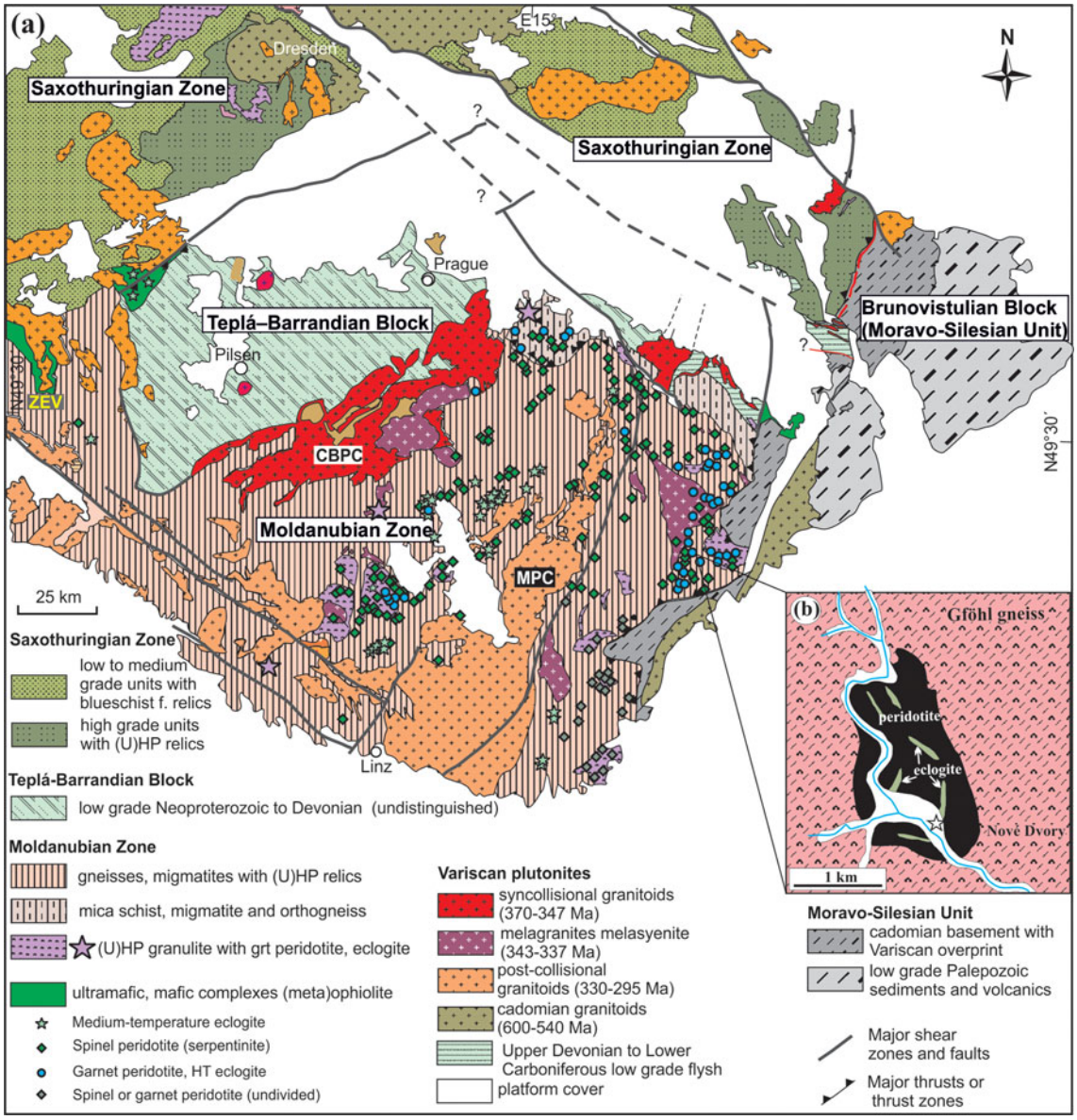

Fig. 1. (*a*) Simplified geological map of the Bohemian Massif, modified after Cháb *et al.* (2007) and Faryad and Kachlík (2013). CBPC = Central Bohemian Plutonic Complex, MPC = Moldanubian Plutonic Complex. (*b*) Detail of garnet peridotite body with eclogite in Nové Dvory. The open star indicates the location of the sample from the eclogite body with apatite.

intruded by late Variscan granitoid plutons in its western and central parts. The garnet peridotite blocks reach up to 2 km x 4 km in size and occur sporadically within granulites and migmatitic gneisses (e.g. Medaris *et al.*, 1990). They may contain lenses and layers of eclogite and garnet pyroxenite. The garnet peridotite is lherzolite, harzburgite and rarely dunite in composition and has been extensively affected by serpentinisation.

Ultra-high pressure conditions for both garnet peridotites (5.5 GPa / 1100°C) and eclogites (5 GPa / 1000°C) were estimated by Medaris *et al.* (1990) and Nakamura *et al.* (2004), respectively. Faryad *et al.* (2009) studied exsolution lamellae of garnet in clinopyroxene from clinopyroxenite within garnet peridotite. On the basis of textural and compositional relations they concluded that fragments of original mantle wedge peridotite with lenses and layers of mafic rocks (Medaris *et al.*, 1990; Svojtka *et al.*, 2016) were incorporated in crustal rocks during subduction, shared the same *P-T* trajectory to peak pressure and were exhumed to the surface (Faryad *et al.*, 2018). Recent studies (Perraki and Faryad, 2014; Jedlicka *et al.*, 2015) indicated that the peak pressures were reached by the rocks at a lower temperature (650–800°C) than that (1200–1300°C) estimated by Medaris *et al.* (1990) and Nakamura *et al.* (2004) and the granulite-facies metamorphism (850–950°C / 1.0–1.6 GPa) occurred after partial exhumation of the UHP rocks into the lower and/or middle crustal levels. This high-temperature granulite-facies overprint resulted from mantle upwelling that occurred due to slab breakoff during a collision orogeny (Faryad *et al.*, 2015).

The garnet peridotite body at Nové Dvory is serpentinised garnet lherzolite (Medaris *et al.*, 1990) within migmatitic and granulite gneisses (Fig. 1*b*). It contains several large (up to 500 m long) lenses of eclogite (Fig. 1*b*) and thin layers of clinopyroxenite. On the basis of their geochemistry the lenses and layers of mafic rocks

https://doi.org/10.1180/mgm.2018.146 Published online by Cambridge University Press

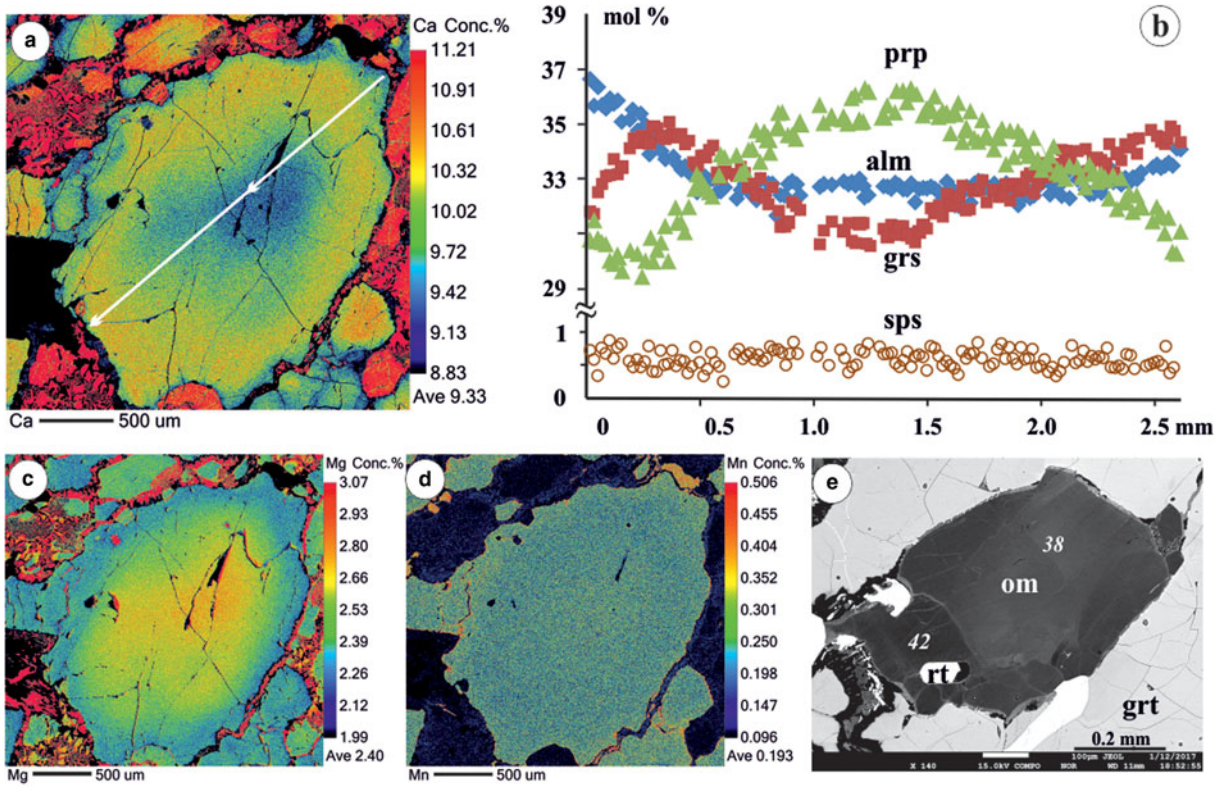

Fig. 2. False-colour compositional maps of garnet (*a*, *c*, *d*) with qualitative concentration of elements in wt.% and profile (*b*) which shows the zoning pattern (in mol.%) of pyrope (prp), almandine (alm), grossular (grs) and spessartine (sps). (e) BSE image of compositionally zoned omphacite with dark and light domains having different jadeite contents (in mol.%). Omphacite contains rutile (rt) inclusions and at the rim is replaced by a symplectite of plagioclase + amphibole + diopside).

with peridotite formed by melt that migrated through the lithospheric mantle wedge above the subduction zone (Medaris *et al.*, 2006; Ackerman *et al.*, 2009). Exsolution lamellae of garnet in clinopyroxene from clinopyroxenite layers were investigated by Faryad *et al.* (2009) who concluded that formation of the lamellae by cooling was when the hot mantle rocks became involved with down-going crustal material during subduction. The eclogite investigated in this present work is exposed in the southern part of the garnet peridotite body as indicated in Fig. 1*b*.

Analytical methods

Compositional data and X-ray mapping were obtained using a JEOL JXA-8530F field-emission gun electron microprobe analyser (FEG-EMPA) equipped with wavelength- and energy-dispersive spectrometers (WDS and EDS) at the Institute of Petrology and Structural Geology, Charles University in Prague. The analyses were performed on polished thin-sections with normal operating conditions for spot and analyses with a defocused beam (5–10 μm wide) with 15 kV and 30 nA beam current and 30 s counting time on peak and total background. Typical detection limits for these analytical conditions were in the range of 50–150 ppm (3σ). The SPI #02753–AB 53 mineral standards were used for following elements: Si (*K*α) – quartz; Al (*K*α) – corundum; Mg (*K*α) – periclase; Fe (*K*α) – magnetite; Mn (*K*α) – rhodonite; Ca (*K*α) – calcite, diopside; Ti (*K*α) – rutile; Cr (K α) – chromium oxide; Na (*K*α) – albite; P (*K*α) – apatite; Ni (*K*α) – nickel oxide; Y (*L*α) – YAG. These elements were measured by the WDS crystals: TAP (Na, Mg, Al, Si, Y, P); PET (Ti, Cr, Ca, V); LIF (Mn, Fe, Ni). The ZAF algorithm was applied for correction of raw data. The same method was applied for detailed compositional profiles of major and trace elements. For high-resolution compositional mapping of major and trace elements, analytical conditions of 20 kV and 120 nA were used. The rare-earth elements (*REE*), As, Sr, F, Cl and S, detected in apatite and its exsolutions, were measured quantitatively only by WDS.

The Raman spectra of lamellae in apatites were obtained with a Renishaw Ramascope RM1000® Raman micro-spectrometer at the School of Mining and Metallurgical Engineering of the Technical University of Athens, Greece. Spectra were excited at room temperature with the 632.8 nm line of a red 19 mW He–Ne laser through an OLYMPUS® ×100 objective. The numerical aperture of the objective is 0.9. The laser spot on the surface has a diameter of ~1 μm and a power of 4 mW. The entrance slit into the spectrometer was set to 4 μm. Light was dispersed by a holographic grating with 1800 grooves/mm. Three accumulations of 20 s each were made to provide a good signal-to-noise ratio. The wavenumber calibration was checked regularly by measuring the position of the Rayleigh line and the LO phonon mode of a silicon single-crystal wafer.

Petrology

The eclogite with apatite is medium-to-coarse grained with garnet porphyroblasts between 1 and 3 mm in size and locally up to 8 mm. It is weakly foliated and in addition to garnet (up to 70 vol.% of the rock) contains omphacite and accessory amounts of amphibole, biotite, K-feldspar, ilmenite, rutile, apatite and

https://doi.org/10.1180/mgm.2018.146 Published online by Cambridge University Press

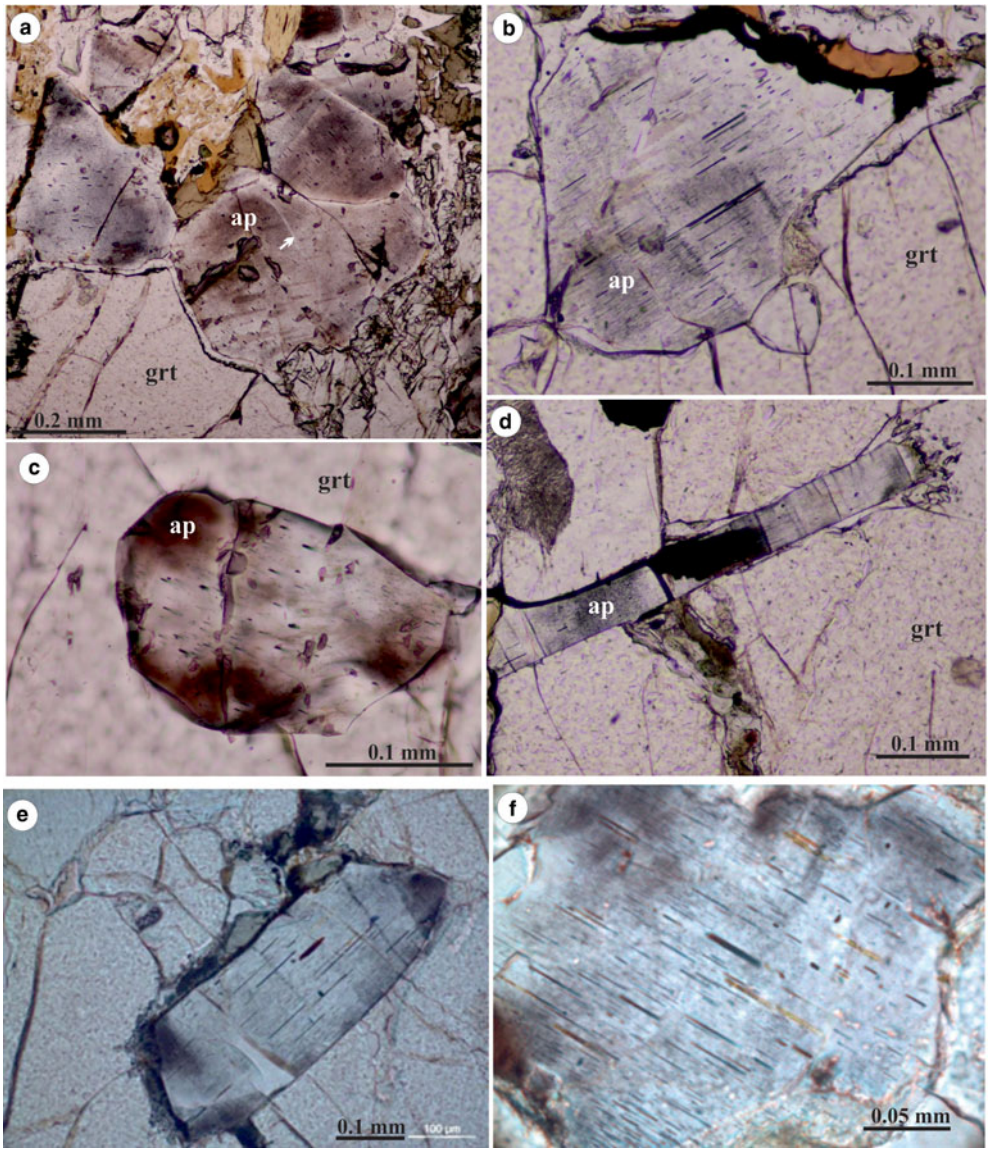

Fig. 3. Plane polarised light images. Apatite (ap) forming clusters (*a*) or separate grains as inclusions (*c–f*) in garnet (grt). Note parallel inclusion patterns and variously shaded domains in a single grain of apatite. The white arrow in (*a*) indicates an exsolution-free track (probably healed fractures).

spinel. Omphacite is relatively fresh and it is replaced partly by a very fine-grained symplectite of plagioclase, diopside and/or an amphibole. In contact with garnet, it is rimmed by green amphibole. Brown amphibole is present at the contact with ilmenite. The amphibole is partly replaced by biotite. Biotite with green spinel forms pseudomorphs after an unknown phase (probably phengite). In some cases, the boundaries between minerals are formed by thin coronae with symplectite of amphibole (?) and plagioclase and the fine grains in the symplectite have an orientation perpendicular to the interface of garnet and/or omphacite. Rutile is rarely present in garnet, but that occurring in the intergranular spaces between garnet and omphacite is rimmed or totally replaced by ilmenite.

Garnet from eclogite is zoned with high pyrope contents (*ca.* 36 mol.%) in the core which decrease towards the mantle before increasing at the outermost part of the rim (Fig. 2). Both almandine and grossular components show an increase towards the rims, but grossular additionally shows a decrease at the outermost part of the rim. Spessartine content is very low (~0.6 mol.%) and shows an almost flat compositional profile. The decrease in pyrope and increase in grossular content from core to the mantle part of garnet indicates a temperature decrease and pressure increase as result of the exchange reaction between garnet and clinopyroxene (Ellis and Green, 1979), the process similar to that described for formation of the exsolution lamellae in clinopyroxene from clinopyroxenite (Faryad *et al.*, 2009). This differs from subduction of cold crustal rocks heated by pressure increase during subduction and show increase of both Mg and Ca towards the rims (Jedlicka *et al.*, 2015). The increase in pyrope and decrease in grossular at the outermost rim part of garnet (Fig. 2) signify granulite-facies metamorphism occurring at lower pressure. The low grossular content is due to stabilisation of plagioclase in granulite-facies conditions.

Omphacite has a jadeite content up to 42 mol.%. The ferrous and ferric iron contents were calculated by stoichiometric and charge-balance criteria. Compositional maps of some omphacite grains show zoning with slightly jadeite-rich domains at the rims (Fig. 2*e*). Omphacite shows a thin diffusion rim with small

https://doi.org/10.1180/mgm.2018.146 Published online by Cambridge University Press

Table 1. Representative compositions from microprobe analyses of apatite from eclogite in the Nové Dvory.

	Apatite		Inclusions in garnet	
Constituent	Matrix	Matrix	Dark	Light
Wt.%				
P_2O_5	41.34	40.72	41.22	40.9
SiO_2	0.13	0.83	0.14	0.15
Nd_2O_3	0.06	bdl	0.10	0.13
Ce_2O_3	0.11	0.05	0.04	0.18
La_2O_3	0.05	0.04	0.06	0.10
FeO	0.47	0.87	0.66	0.13
MnO	0.05	0.02	b.d.l	b.d.l
MgO	0.11	0.33	0.08	0.06
NiO	0.13	b.d.l	0.02	b.d.l
As_2O_5	0.20	b.d.l	b.d.l	b.d.l
CaO	54.99	54.02	54.62	54.29
SrO	b.d.l	0.22	0.50	0.48
Na_2O	0.19	0.13	0.22	0.15
SO_3	0.53	0.21	0.81	0.23
F	2.25	2.24	2.25	2.31
Cl	0.39	0.28	0.33	0.27
Total	100.98	100.02	101.08	99.37
O = F,Cl	0.672	0.623	0.647	0.635
Total	100.30	99.40	100.43	98.74
Atoms per formula unit based on 25 oxygens				
P	5.867	5.832	5.848	5.914
Si	0.021	0.14	0.023	0.026
Nd	0.004		0.006	0.008
Ce	0.006	0.003	0.003	0.011
La	0.003	0.003	0.004	0.006
Fe	0.065	0.124	0.093	0.018
Mn	0.007	0.003		
Mg	0.028	0.084	0.019	0.014
Ni	0.017		0.003	
As	0.017			
Ca	9.877	9.793	9.805	9.933
Sr		0.021	0.049	0.047
Na	0.06	0.041	0.071	0.049
S	0.067	0.026	0.101	0.029
F	1.135	1.138	1.135	1.183
Cl	0.105	0.077	0.088	0.075
Total	17.28	17.291	17.252	17.314

bdl – below the detection limit.

amounts of jadeite. The amphibole is pargasite in composition and occurs in the intergranular spaces; some relic grains have rutile needles.

Apatite and exsolved minerals

Apatite is a common phase in the rock, occurring in the matrix and also as inclusions in garnet and omphacite. It forms clusters or separate grains with euhedral- to- subhedral habits and is up to 1 mm x 0.3 mm in size (Fig. 3). In polarised-light microscopy the grains appear to have domains, visible as fine dusty particles. The modal abundance of apatite in the rock is ~1 vol.%. The apatite contains F (2–3 wt.%) and has a maximum Cl content of 0.4 wt.% (Table 1).

Apatite contains very fine needle-like lamellae, and in rare cases, rods, that are oriented crystallographically parallel to the *c* axis (determined by polarised-light microscopy). Together with the fine particles, they give a dusty appearance to the apatite grains (Figs 3 and 4). The particles are very small and their non-linear shapes on the surface could be due to the orientation of apatite grains (not parallel to the crystallographic planes). When comparing microphotographs and cathodoluminescence (CL) images, the dusty domains match a CL response with different intensity of luminescence (Fig. 5); the dusty domains have sharp boundaries with lower luminescence in the CL images. X-ray maps of apatite grains (Fig. 6) indicate that the dusty domains have a high concentration of Fe and S. No relation between F or Cl distribution and dusty domains in apatite (Fig. 6*d*, *e*) was observed. Plane-polarised-light microphotographs (Fig. 6*a*) and X-ray maps of S and Fe (Fig. 6*b*, *c*) indicate exsolution free tracks that probably represent former fractures in apatite crystals that were later healed. Some of these healed fractures (Fig. 5*c*) are also visible in CL images (Fig. 5*f*).

Oriented lamellae and rods in apatite

Microphotographs and back-scatter electron (BSE) images (Figs 3 and 4) indicate that, in addition to dusty particles, relatively large oriented rods and lamellae are present. Detailed Raman spectroscopy and microprobe analyses indicated that they represent various mineral phases. As the phases are very small, the true composition is difficult to determine, but by a combination of all these methods, five types of inclusions were observed. They are: (1) Fe sulfide; (2) Cu–Fe sulfide; (3) Ni–Co–Fe sulfide; (4) Fe oxide; and (5) baryte (Figs 7 and 8). Because of the small size of the lamellae, most analyses contain P and Ca from the host apatite. In such cases, P and Ca structurally bound to apatite were subtracted from the analyses to determine the composition of the lamellae. Most of the inclusions are rich in Fe. They generally form lamellae (Fig. 7*b*), but some polyhedral grains are also present (Fig. 7*e*). In addition to almost pure Fe oxide, Fe sulfide was also analysed. It has higher Fe content than common natural sulfide minerals (FeS, FeS_2). On the basis of normalised Fe and S contents ($Fe_{6.80}S_{8.19}$), it is close to monoclinic pyrrhotite (Fe_7S_8). In addition to S, some lamellae contain Cu that range from 5.37 to 28.81 wt.% and minor Ni and Co. The high Cu content in the lamellae probably indicates the presence of other phases such as chalcopyrite, pentlandite or possible solid solutions between two phases. The sulfide and baryte lamellae were also identified from Raman spectra (Fig. 8). The best data (without excitation of the host apatite) were obtained for the large baryte lamellae. This has a small amount of Sr ($Ba_{0.979}Sr_{0.066}S_{0.985}O_4$) or Ca ($Ba_{0.973}Ca_{0.066}S_{0.999}O_4$) (Table 2). Both baryte and sulfide lamellae occur in a single apatite grain.

Discussion

Relationship between density of exsolved phases and compositional zoning in apatite

Microphotographs indicate that the lamellae and submicroscopic (dusty) exsolutions are not distributed regularly throughout the apatite crystals and show no relation to the core or rim of grains. Similarly, no relationship was found in the density and distribution of the exsolved phases between the apatite grains forming inclusions in garnet or omphacite and those occurring in the matrix. However, a combination of optical microscopy with compositional mapping revealed that the dusty domains have high concentrations of Fe, S and other elements (Fig. 6*a*–*c*). Because of the very small sizes of the dusty particles, it was not possible to determine if the high concentrations of Fe and S observed in the maps are only from the fine particles or also from the host apatite. Detailed microprobe analyses of relatively large lamellae show a wide range of composition that includes variable amounts of Fe, S, Sr, Cu, Ni, Co, Al, Ba and Mg. The contents of P, Ca, F

https://doi.org/10.1180/mgm.2018.146 Published online by Cambridge University Press

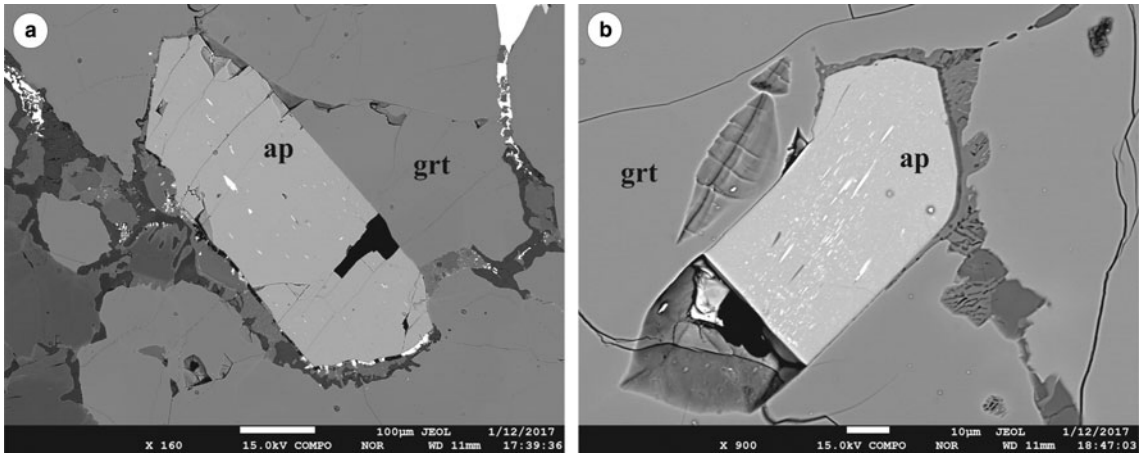

Fig. 4. BSE images of apatite inclusions in garnet. Note that the lamellae of different sizes in apatite are oriented parallel to the *c* axes of crystals. The black areas are holes created during sample preparation. (*a*) Scale bar = 100 μm; (*b*) scale bar = 10 μm.

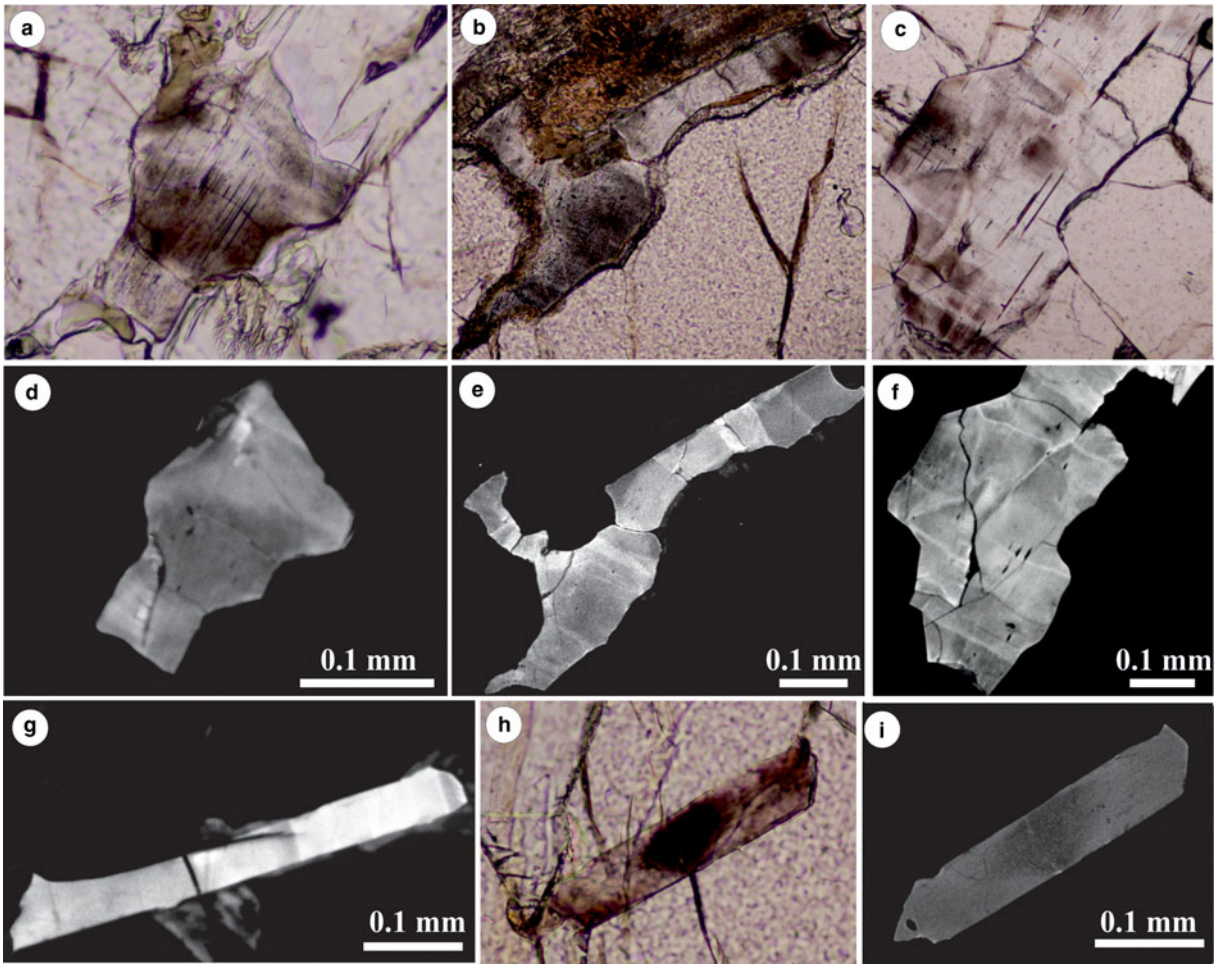

Fig. 5. Microphotographs (*a*, *b*, *c*, *h*) and respective cathodoluminescence (CL) images (*d*, *e*, *f*, *g*, *i*) of dusty domains in apatite. Note that the areas of high concentration of dusty domains show a lower luminescence intensity in CL images. Some domains have a sharp boundary and appear as sector zoning of the apatite crystals.

and Cl in the analysis of the small inclusions originate from the host apatite. Pan and Fleet (2002) and Hughes and Rakovan (2015) note that all these elements are common in apatite-supergroup minerals. According to the International Mineralogical Association Commission on New Minerals, Nomenclature and Classification nomenclature (Pasero *et al.*, 2010) the apatite supergroup contains five groups: apatite, belovite, britholite, ellestadite and hedyphanite. Most of the elements

https://doi.org/10.1180/mgm.2018.146 Published online by Cambridge University Press

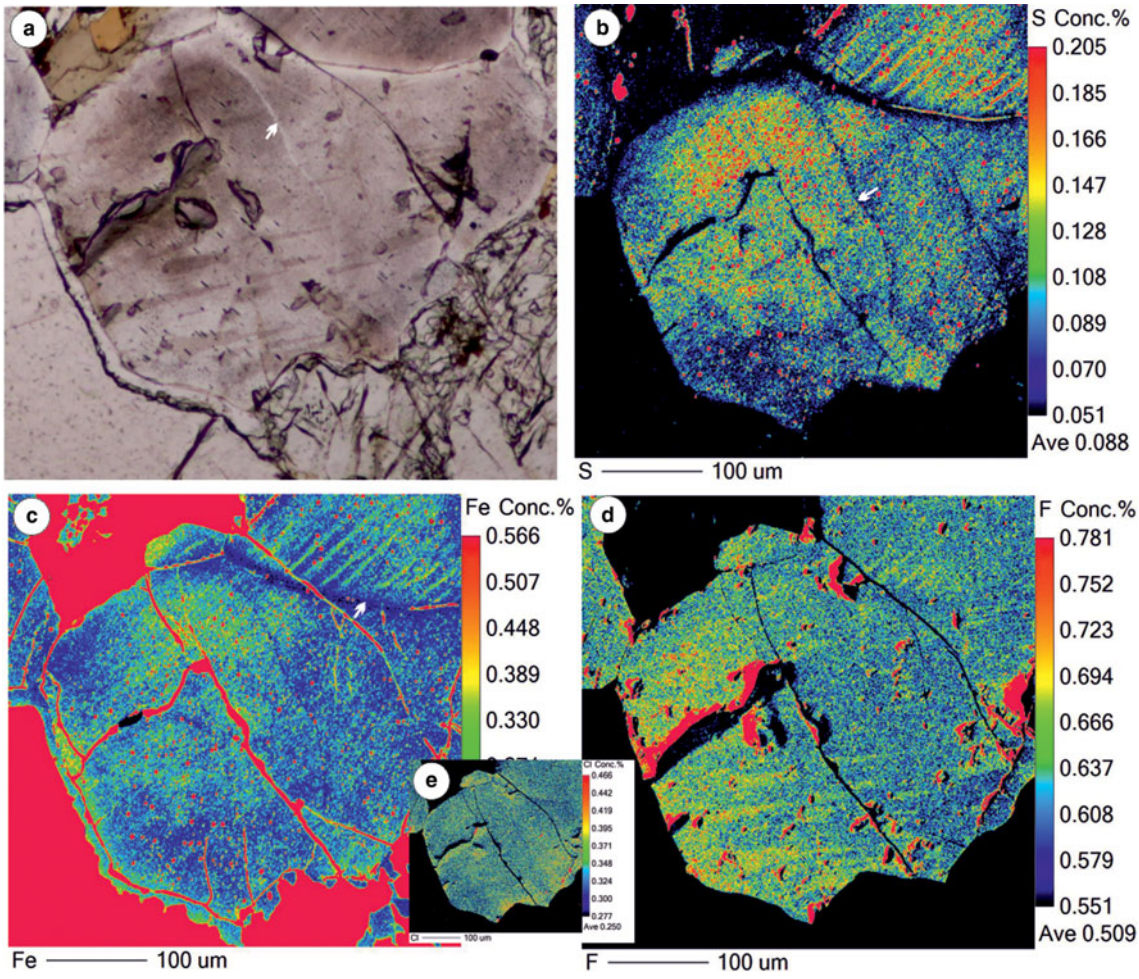

Fig. 6. Apatite with an inclusion of dusty domains (*a*) and corresponding false-colour compositional maps (qualitative concentration of elements in wt.%) of S (*b*), Fe (*c*), F (*d*) and Cl (*e*, inset). Note that domains with high concentration of inclusions have high Fe and S contents. The white arrows in (*a*), (*b*) and (*c*) indicate exsolution-free tracks.

(Ca, Sr, Ba, Fe, Cu, Co, Ni and Mg) occupy the *M*1 and *M*2 sites of the apatite crystal structure, while P, S and Si are positioned in the tetrahedral (*T*) site. Fluorapatite, chlorapatite and hydroxylapatite ($M1 = M2 = Ca$, $T = P$) are most common in the apatite-group minerals and in addition to Ca and P, they may contain Ba, Pb, As, Mn, Sr and V. Other groups, e.g. the belovite and britholite groups may incorporate Ce, Sr, Nd, Y, Na, Ba or B and those of the ellestadite and hedyphanite groups can contain Si, S, Pb, Na, Bi, As and Ba.

Another observation from the apatite microtextures is the relationship between dusty domains with a high density of exsolutions and sector zoning. The dusty domains with high concentrations of Fe and S are only developed in some sectors. This is consistent with the observation of Rakovan (2002), suggesting that, in addition to a number of factors, the crystal growth of apatite is controlled by surface structural and chemical effects. A very close relationship was found between the concentration of *REE*, mainly La, Sm, Nd, etc. and sector zoning in apatite (Rakovan and Reeder, 1996). Therefore, the surface of an apatite crystal defines the interface with surroundings that may have very different characteristics at the contact with other phases. We assume that the sector zoning in apatite was developed, similar to that noted in other minerals (e.g. tourmaline, Van Hinsberg *et al.*, 2006), by preferential uptake of elements on the growth planes, resulting from a combined effect of differences in surface charge and morphology of these planes.

Origin and formation of the exsolution lamellae

According to Harlov *et al.* (2002) and Harlov (2015), variation of trace-element concentrations in apatite could be mostly a result of metasomatic processes. They studied partially metasomatised chlorapatite from Ødegårdens Verk in Norway and experimentally investigated metasomatised apatite in an H_2O- and F-rich system. On the basis of their BSE images, of natural apatite and experimental products (Harlov *et al.*, 2002), the apatite grains have clearly reacted along their rims or been pervasively penetrated by reaction fronts. The study found that the reacted areas with high F and OH contents were depleted in *REE*, which is explained to be a result of 'chlorapatite' replacement by OH- and fluorapatite. A metasomatic origin for the exsolution lamellae in apatite was also adopted by Broska *et al.* (2014), who investigated pyrrhotite, anhydrite and dolomite oriented rods in apatite in silicate-bearing carbonate rocks associated with UHP eclogites in the Tromsø Nappe of the Scandinavian Caledonides in Norway. They considered the lamellae formed in a fluid-aided

https://doi.org/10.1180/mgm.2018.146 Published online by Cambridge University Press

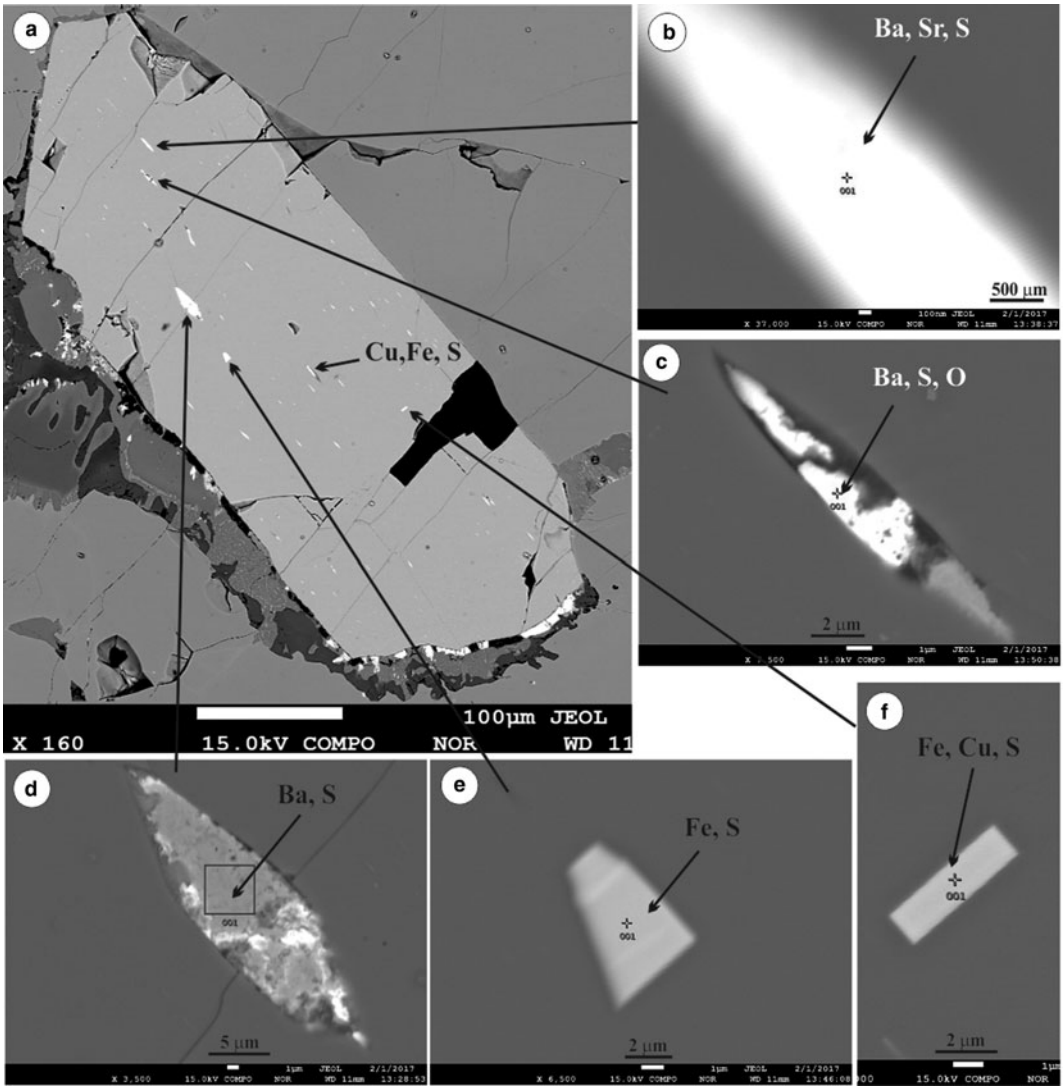

Fig. 7. BSE images of apatite crystal (*a*) with exsolution lamellae of baryte (*b–d*) and Fe, Cu sulfides (*e* and *f*). Note that some, relatively large inclusions (*c* and *d*) are multiphase. The BSE image in (*a*) is from that in Fig 3e. The crosses and squares are positions from where analyses and spectra were acquired.

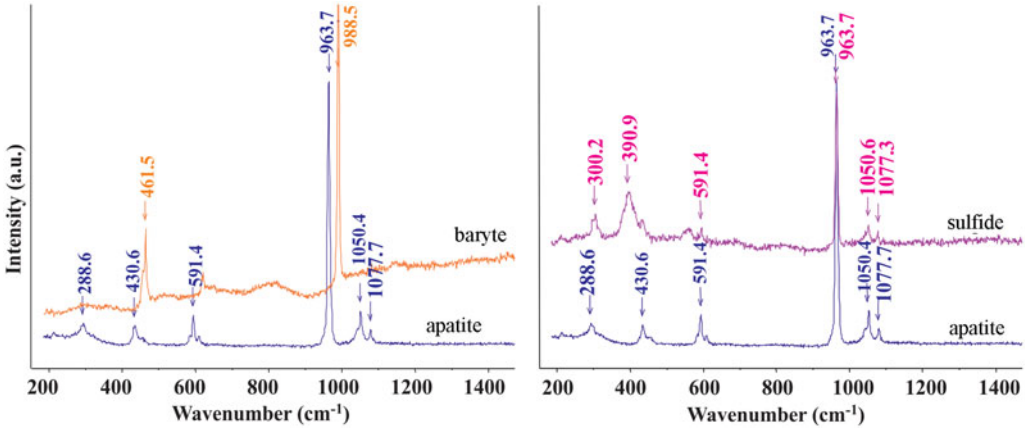

Fig. 8. Raman spectra of baryte and sulfide lamellae in apatite. The sulfide lamella analysed is indicated in Fig. 7a (Cu, Fe, S).

regime during amphibolite-facies metamorphism, subsequent to the UHP event.

In contrast to metasomatised apatite with replacement along the rims and penetrative zones by Harlov *et al.* (2002, 2015), we observed no relationship between the concentration of cations and fluorine or chlorine contents. In addition, concentration of the exsolution lamellae or dusty domains correlate well with the high trace-element concentration in the compositional

https://doi.org/10.1180/mgm.2018.146 Published online by Cambridge University Press

Table 2. Representative compositions from microprobe analysis of lamellae in apatite.

	Baryte			Fe sulfide			Fe–Cu sulfides		
Wt.%									
SrO	2.90	b.d.l.	Fe	59.12	58.16	Cu	5.37	7.15	28.81
BaO	63.68	63.21	S	40.88	41.84	Fe	58.39	56.67	36.01
CaO	0.00	1.62	Total	100.00	100.00	S	6.29	36.17	35.18
SO_3	33.43	35.17				Total	100.00	100.00	100.00
Total	100.00	100.00							
Atoms per formula unit									
No. of cations	4	4	No. of ions	15	15	No. of ions	15	15	4
Sr	0.066		Fe	6.804	6.657	Cu	0.560	0.751	0.825
Ba	0.979	0.973	S	8.195	8.342	Fe	6.934	6.749	1.175
Ca	0.000	0.066				S	7.507	7.500	2.000
S	0.985	0.999							

b.d.l. = below detection limit.

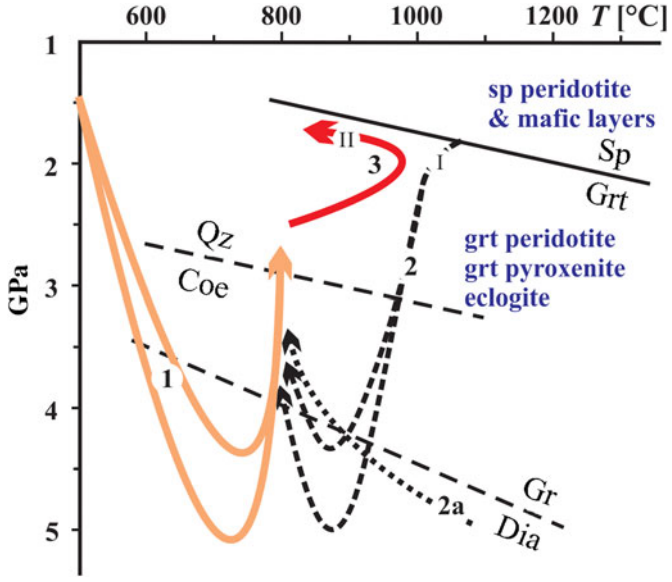

Fig. 9. Schematic diagram showing *P-T* paths of eclogite and host garnet peridotite and granulite (Faryad *et al.*, 2018). (1) Indicates subduction of felsic crustal rocks (now granulite) that took hot (or partially cooled fragments, due to the subduction geotherm) mantle peridotite with lenses and layers of mafic rocks which cooled down during pressure increase (2). Path (2a) shows involvement of mantle rock at maximum depths. After exhumation of crustal and mantle rocks to crustal levels, they underwent granulite-facies metamorphism (3) that was a result of slab break-off and mantle upwelling. (I) and (II) indicate possible crystallisation of apatite and formation of exsolution lamellae in apatite, respectively. Mineral abbreviations are: coe – coesite, dia – diamond, gr – graphite, grt – garnet, qz – quartz, sp – spinel.

maps (Fig. 6). We assume therefore that the elements present in the exsolution lamellae or identified in the compositional maps are the original impurities in the apatite crystal structure (Hughes and Rakovan, 2015). Both lamellae and fine particles were then formed by exsolution in a closed system and originated from the original impurities in the apatite crystal. As shown by Parsons and Brown (1991), the process of unmixing of a single-phase solid solution into a two-phase assemblage is driven by free-energy minimisation and occurs by diffusion. Once two phases become established, the exsolution microtexture coarsens with time, also by diffusion. This seems to be the reason for the presence of fine particle exsolutions in the apatite crystals studied.

Formation of apatite and exsolutions in relation to the metamorphic P-T path of the host eclogite

Considering the eclogite and host garnet peridotite in Nové Dvory are fragments of subcontinental lithospheric mantle (Medaris *et al.*, 2006; Ackerman *et al.*, 2009) and that they were recrystallized during subduction (Faryad *et al.*, 2009; 2013*b*), it is needed to clarify textural relations of apatite to other HP-UHP phases before the formation of apatite and exsolved inclusions is discussed. The occurrence of apatite within garnet and omphacite, even in central parts of the grains, indicates it is either a relic phase or crystallised during garnet and omphacite formation. In both cases, it could be formed by interaction of fluids generated in a subduction zone and infiltrated into the hot mantle wedge (Fig. 9). As shown by many experimental studies (Watson and Green, 1981; Fleet and Pan, 1997; Prowatke and Klemme, 2006), the incorporation of trace elements in apatite is, in addition to partition coefficients of the elements, controlled by their abundance in a melt or in fluid and by temperature changes. It is therefore probable that apatite, having such a high concentration of trace elements, formed at relatively high temperatures, when the mantle rocks were incorporated into subduction as it is assumed from the garnet zoning.

The formation of exsolution lamellae in apatite could occur either during cooling or decompression of the host rocks. In most minerals, exsolution occur upon cooling below the temperature of mutual solubility or stability of the solution, but they could be also occur during decompression. The presence of pyrrhotite and other phases in apatite from many granitoids (e.g. Gottesmann and Wirth, 1997; Krneta *et al.*, 2016) is explained by cooling rather than by pressure decrease. The formation of sulfide exsolution lamellae in apatite from some UHP rocks are assumed to be a result of decompression (Chen *et al.*, 2006; Zeng *et al.*, 2006; Sun *et al.*, 2007). The mechanism of exsolution is assumed to be similar to that in other minerals, e.g. quartz and K-feldspar lamellae in clinopyroxene or clinopyroxene exsolution in garnet, which are reported from UHP rocks (Zhang and Liou, 1999; Katayama *et al.*, 2000; Dobrzhinetskaya *et al.*, 2002; Zhang *et al.*, 2005). Decompression-derived quartz or coesite lamellae are explained by the stabilisation of the Ca-Eskola component at high-pressure conditions (Gasparik, 2003; Zhao *et al.*, 2011). However, the exsolution mechanism of sulfides and other phases in apatite during decompression has not yet been satisfactorily explained.

https://doi.org/10.1180/mgm.2018.146 Published online by Cambridge University Press

We do not exclude exsolution in apatite during decompression (exhumation), but for the case of their origin by cooling, two scenarios exist in regard to the above mentioned *P–T* path of the host rocks. The first is their formation in the subduction zone (I in Fig. 9), just after the apatite was formed by the interaction of subduction fluids with hot mantle. The second is that the exsolution occurred during rapid cooling from granulite-facies metamorphism (II in Fig. 9) in crustal levels. A short-lived granulite-facies metamorphism in the Moldanubian Zone was confirmed by the preservation of prograde zoning in felsic granulite (Jedlicka *et al.*, 2015) and by recrystallisation of retrograde phases formed in the cracks of eclogite-facies garnet into granulite-facies assemblages (Faryad and Fišera, 2015). In the case of exsolution formation during cooling from the peak temperatures in granulite-facies conditions, the tracks after former cracks (Figs 3*a*, 5*c*,*f* and 6*b*,*c*) could also be healed during granulite-facies metamorphism.

Acknowledgements. This work was supported by the Czech Science Foundation (research project number 18-03160S), the Charles University (project GA UK no. 84217) and by institutional project Progres Q45. We thank H.-P Schertl and an anonymous reviewer for very helpful reviews. M. Arima is thanked for editorial handling.

References

Ackerman L., Jelínek E., Medaris G., Ježek J., Siebel W. and Strnad L. (2009) Geochemistry of Fe-rich peridotites and associated pyroxenites from Horní Bory, Bohemian Massif: Insights into subduction-related melt-rock reactions. *Chemical Geology*, **259**, 152–167.

Broska I., Krogh Ravna E.J., Vojtko P., Janák M., Konečný P., Pentrák M., Bačík P., Luptáková J. and Kullerud K. (2014) Oriented inclusions in apatite in a post-UHP fluid-mediated regime (Tromsø Nappe, Norway). *European Journal of Mineralogy*, **26**, 623–634.

Cháb J., Stráník Z. and Eliáš M. (2007) *Geologická mapa České republiky 1:500.000*. Česká geologická služba.

Chen J., Zeng L.S., Chen F.Y. and Liang F.H. (2006) Primary study of exsolution in apatite from the Qinglongshan, Jiangsu Province. *Acta Petrologica Sinica*, **22**, 1921–1926 [in Chinese].

Cherniak D.J. (2000) Rare earth element diffusion in apatite. *Geochimica et Cosmochimica Acta*, **64**, 3871–3885.

Dobrzhinetskaya L.F., Schweinehage R., Massonne H.J. and Green H.W. (2002) Silica precipitates in omphacite from eclogite at Alpe Arami, Switzerland: evidence of deep subduction. *Journal of Metamorphic Geology*, **20**, 481–492.

Ellis D.J. and Green D.H. (1979). An experimental study of the effect of Ca upon garnet-clinopyroxene Fe--Mg exchange equilibria. *Contributions to Mineralogy and Petrololgy*, **71**, 13–22.

Faryad S.W. and Fišera M. (2015) Olivine-bearing symplectites in fractured garnet from eclogite, Moldanubian Zone (Bohemian Massif) – a short-lived, granulite facies event. *Journal of Metamorphic Geology*, **33**, 597–612.

Faryad S.W. and Kachlík V. (2013) New evidence of blueschist facies rocks and their geotectonic implication for Variscan suture(s) in the Bohemian Massif. *Journal of Metamorphic Geology*, **31**, 63–82.

Faryad S.W., Dolejš D. and Machek M. (2009) Garnet exsolution in pyroxene from clinopyroxenites in the Moldanubian zone: constraining the early pre-convergence history of ultramafic rocks in the Variscan orogen. *Journal of Metamorphic Geology*, **27**, 655–671.

Faryad S.W., Jedlicka R. and Ettinger K. (2013*a*) Subduction of lithospheric upper mantle recorded by solid phase inclusions and compositional zoning in garnet: example from the Bohemian Massif. *Gondwana Research*, **23**, 944–955.

Faryad S.W., Jedlicka R. and Collett S. (2013*b*) Eclogite facies rocks of the Monotonous unit, clue to Variscan suture in the Moldanubian Zone (Bohemian Massif). *Lithos*, **179**, 353–363.

Faryad S.W., Kachlík V., Sláma J. and Hoinkes G. (2015) Implication of corona formation in a metatroctolite to the granulite facies overprint of HP-UHP rocks in the Moldanubian Zone (Bohemian Massif). *Journal of Metamorphic Geology*, **33**, 295–310.

Faryad S.W., Jedlicka R., Hauzenberger C. and Racek M. (2018) High-pressure crystallization vs. recrystallization origin of garnet pyroxenite-eclogite within subduction related lithologies. *Mineralogy and Petrology*, **112**, 603–616.

Fleet M.E. and Pan Y.M. (1997) Site preference of rare earth elements in fluorapatite: binary (LREE + HREE)-substituted crystals. *American Mineralogist*, **82**, 870–877.

Gasparik T. (2003) *Phase Diagrams for Geoscientists. An Atlas of the Earth's Interior*. Springer, 462 pp.

Gottesmann B. and Wirth R. (1997) Pyrrhotite inclusions in dark pigmented apatite from granitic rocks. *European Journal of Mineralogy*, **9**, 491–500.

Harlov D.E. (2015) Apatite: a fingerprint for metasomatic processes. *Elements*, **11**, 171–176.

Harlov D.E., Förster H.J. and Nijland T.G. (2002) Fluid-induced nucleation of (Y + REE)-phosphate minerals within apatite: Nature and experiment. Part I. Chlorapatite. *American Mineralogist*, **87**, 245–261.

Hughes J.M. and Rakovan J.F. (2015) Structurally robust, chemically diverse: apatite and apatite supergroup minerals. *Elements*, **11**, 165–170.

Jedlicka R., Faryad S.W. and Hauzenberger C. (2015) Prograde metamorphic history of UHP granulites from the Moldanubian Zone (Bohemian Massif) revealed by major element and Y + REE zoning in garnets. *Journal of Petrology*, **56**, 2069–2088.

Katayama I., Patkinson C.D., Okamoto K., Nakajima Y. and Maruyama S. (2000) Supersilicic clinopyroxene and silica exsolution in UHPM eclogite and pelitic gneiss from the Kokchetav massif, Kazakhstan. *American Mineralogist*, **85**, 1368–1374.

Korzhinsky M.A. (1981) Apatite solid solutions as indicators of the fugacity of HCl and HF in hydrothermal fluids. *Geochemistry International*, **3**, 45–60.

Krneta S., Ciobanu C.L., Cook N.J., Ehrig K. and Kontonikas-Charos A. (2016) Apatite at Olympic Dam, South Australia: A petrogenetic tool. *Lithos*, **262**, 470–485.

Liou J.G., Zhang R.V., Ernst W.G., Rumble D.I. and Maruyama S. (1998) High-pressure minerals from deeply subducted metamorphic rocks. Pp. 33–96 in: *Ultrahigh Pressure Mineralogy: Physics and Chemistry of the Earth's Deep Interior* (R.J. Hemley, editor). Reviews in Mineralogy, 37. Mineralogical Society of America, Washington, DC.

Liu L., Yang J., Zhang J., Chen D., Wang C. and Yang W. (2009) Exsolution microstructures in ultrahigh-pressure rocks: Progress, controversies and challenges. *Chinese Science Bulletin*, **54**, 1983.

Medaris L.G., Wang H.F., Mísař Z. and Jelínek E. (1990) Thermobarometry, diffusion modelling and cooling rates of crustal garnet peridotites: two examples from the Moldanubian zone of the Bohemian Massif. *Lithos*, **25**, 189–202.

Medaris L.G., Beard B.L. and Jelínek E. (2006) Mantle-derived, UHP garnet pyroxenite and eclogite in the Moldanubian Gföhl Nappe, Bohemian Massif: a geochemical review, new P–T determinations, and tectonic interpretation. *International Geology Review*, **48**, 765–777.

Nakamura D., Svojtka M. and Naemura K. (2004) Very high-pressure (>4 GPa) eclogite associated with the Moldanubian zone garnet peridotite (Nové Dvory, Czech Republic). *Journal of Metamorphic Geology*, **22**, 593–603.

Pan Y. and Fleet M.E. (2002) Compositions of the apatite-group minerals: substitution mechanisms and controlling factors. Pp. 13–49 in: *Phosphates* (M.L. Kohn, J. Rakovan and J.M. Hughes, editors). Reviews in Mineralogy and Geochemistry, **48**. Mineralogical Society of America and the Geochemical Society, Chantilly, Virginia, USA.

Parsons I. and Brown W.L. (1991) Mechanisms and kinetics of exsolution-structural control of diffusion and phase behavior in alkali feldspars. Pp. 304–344 in: *Diffusion, Atomic Ordering, and Mass Transport. Advances in Physical Geochemistry* (J. Ganguly, editor). Selected Topics in Geochemistry 8. Springer, New York, NY.

Pasero M., Kampf A.R., Ferraris C., Pekov I.V., Rakovan J. and White T.J. (2010) Nomenclature of the apatite supergroup minerals. *European Journal of Mineralogy*, **22**, 163–179

https://doi.org/10.1180/mgm.2018.146 Published online by Cambridge University Press

Perraki M. and Faryad S.W. (2014) First finding of microdiamond, coesite and other UHP phases in felsic granulites in the Moldanubian Zone: Implications for deep subduction and a revised geodynamic model for Variscan Orogeny in the Bohemian Massif. *Lithos*, **202–203**, 157–166.

Prowatke S. and Klemme S. (2006) Trace element partitioning between apatite and silicate melts. *Geochimica et Cosmochimica Acta*, **70**, 4513–4527.

Rakovan J. (2002) Growth and surface properties of apatite. Pp. 51–86 in: *Phosphates* (M.L. Kohn, J. Rakovan and J.M. Hughes, editors). Reviews in Mineralogy and Geochemistry, **48**. Mineralogical Society of America and the Geochemical Society, Chantilly, Virginia, USA.

Rakovan J. and Reeder R.J. (1996) Intracrystalline rare earth element distributions in apatite: Surface structural influences on incorporation during growth. *Geochimica et Cosmochimica Acta*, **60**, 4435–4445.

Sallet R. (2000) Fluorine as a tool in the petrogenesis of quartz-bearing magmatic associations: applications of an improved F-OH biotite-apatite thermometer grid. *Lithos*, **50**, 241–253.

Schulmann K., Kröner A., Hegner E., Wendt I., Konopásek J., Lexa O. and Štípská P. (2005) Chronological constraints on the pre-orogenic history, burial and exhumation of deep-seated rocks along the eastern margin of the Variscan orogen, Bohemian Massif, Czech Republic. *American Journal of Science*, **305**, 407–448.

Smith M.P. and Yardley B.W.D. (1999) Fluid evolution during metamorphism of the Otago Schist, New Zealand: (II), Influence of detrital apatite on fluid salinity. *Journal of Metamorphic Geology*, **17**, 187–193.

Spear F.S. and Pyle J.M. (2002) Apatite, monazite, and xenotime in metamorphic rocks. Pp. 293–336 in: *Phosphates* (M.L. Kohn, J. Rakovan and J.M. Hughes, editors). Reviews in Mineralogy and Geochemistry, **48**. Mineralogical Society of America and the Geochemical Society, Chantilly, Virginia, USA.

Sun X.M., Tang Q., Sun W.D., Xu L., Zhai W., Liang J.L., Liang Y.H., Shen K., Zhang Z.M., Zhou B. and Wang F.Y. (2007) Monazite, iron oxide and baryte exsolutins in apatite aggregates from CCSD drillhole eclogites and their geological implications. *Geochimica et Cosmochimica Acta*, **71**, 2896–2905.

Svojtka M., Ackerman L., Medaris L.G., Hegner E., Valley J.W., Hirajima T., Jelinek E. and Hrstka T. (2016) Petrological, geochemical and Sr-Nd-O isotopic constraints on the origin of garnet and spinel pyroxenites from the Moldanubian Zone of the Bohemian Massif. *Journal of Petrology*, **57**, 897–920.

Van Hinsberg V.J., Schumacher J.C., Kearns S., Mason P.R.D. and Franz G. (2006) Hourglass sector zonation in metamorphic tourmaline and resultant major and trace-element fractionation. *American Mineralogist*, **91**, 717–728.

Watson E.B. and Green T.H. (1981) Apatite liquid partition-coefficients for the rare-earth elements and strontium. *Earth and Planetary Science Letters*, **56**, 405–421.

Watson E.B. and Harrison T.M. (1984) Accessory minerals and the geochemical evolution of crustal magmatic systems – a summary and prospectus of experimental approaches. *Physics of the Earth and Planetary Interiors*, **35**, 19–30.

Yardley B.W.D. (1985) Apatite composition and fugacities of HF and HCl in metamorphic fluids. *Mineralogical Magazine*, **49**, 77–79.

Yund R.A. and McCallister R.H. 1970. Kinetics and mechanisms of exsolution. *Chemical Geology*, **6**, 5–30.

Zeng L., Chen J., Liang F.H. and Xu Z.Q. (2006) Widespread occurrences of apatites with high density sulfide mineral solid exsolutions in the Sulu eclogites. *Geochimica et Cosmochimica Acta*, **70**, A733.

Zhang L.F., Song S.G., Liou J.G., Ai Y.L. and Li X.P. (2005) Relict coesite exsolution in omphacite from Western Tianshan eclogites, China. *American Mineralogist*, **90**, 181–186.

Zhang R.Y. and Liou J.G. (1999) Exsolution lamellae in minerals from ultrahigh-pressure rocks. *International Geology Review*, **41**, 981–993.

Zhao S., Nee P., Green H.W. and Dobrzhinetskaya L. (2011) Ca-Eskola component in clinopyroxene: Experimental studies at high pressures and high temperatures in multianvil apparatus. *Earth and Planetary Science Letters*, **307**, 517–524.

https://doi.org/10.1180/mgm.2018.146 Published online by Cambridge University Press